### Title
Three-dimensional Green's function for planar rectangular phased dipole arrays




### Journal
Wave Motion, 34(3)

### ISSN
0165-2125



### Authors
Maci, S
Capolino, F
Felsen, LB



### Publication Date
2001-09-01

### DOI
10.1016/s0165-2125(01)00091-9

ELSEVIER

Wave Motion 34 (2001) 263–279

WAVE MOTION

www.elsevier.com/locate/wavemoti

# Three-dimensional Green's function for planar rectangular phased dipole arrays

S. Maci [a,*], F. Capolino [a], L.B. Felsen [b,c,d]

[a] *Department of Information Engineering, University of Siena, Via Roma 56, 53100 Siena, Italy*
[b] *Department of Aerospace and Mechanical Engineering, Boston University, 110 Cummington Street, Boston, MA 02215, USA*
[c] *Department of Electrical and Computer Engineering, Boston University, 110 Cummington Street, Boston, MA 02215, USA*
[d] *University Professor Emeritus, Polytechnic University, Brooklyn, NY 11201, USA*

Received 4 December 2000; accepted 5 March 2001

**Abstract**

This paper deals with the construction, physical interpretation and application of a uniform high-frequency representation of array Green's functions (AGFs) for planar rectangular phased arrays of dipoles. An AGF is the basic constituent for the full-wave description of electromagnetic radiation from large periodic structures. For efficient treatment of high-frequency phenomena, the AGF obtained by direct summation over the contributions from the individual radiators is globally restructured via the Poisson sum formula into a series of propagating and evanescent Floquet waves (FWs) together with corresponding FW-modulated diffracted waves, which arise from FW scattering at the array edges and vertexes. These results are obtained by high-frequency uniform asymptotics applied to the wave integrals generated by Poisson summation in the spatial or spectral domains. The final algorithm is physically appealing, numerically accurate, and efficient, owing to the rapid convergence of both the FW series and the series of corresponding FW-modulated diffracted fields away from the array plane. The use of the asymptotic AGF in the full-wave analysis of large slot arrays is discussed, with the inclusion of numerical results.


## 1. Introduction

Periodic structures are of interest in many current engineering applications, which include phased array antennas [1–10]. In modeling the performance of such structures, one of the main objectives is the reduction of the often prohibitive numerical effort that accompanies an element-by-element full-wave analysis based on integral equations which are structured around the ordinary free space Green's function. For a periodic array, this array Green's function (AGF) is composed of the sum over the individual dipole radiations. As an alternative, we explore replacement of the element-by-element Green's function by a global AGF which is constructed via Poisson summation and represents, in terms of the resulting Poisson-transformed integrals, the collective field radiated by the elementary dipoles. Applying high-frequency asymptotics, the radiation from, or scattering by, finite phased arrays is interpreted as the radiation from a superposition of continuous equivalent Floquet wave (FW)-matched source distributions extending over the entire finite array aperture, from which the FW-based AGF can be calculated efficiently. This approach has been applied successfully to various prototypical configurations, such as linear arrays of dipoles [3], arrays of line sources

* Corresponding author.
*E-mail address:* macis@ing.unisi.it (S. Maci).

0165-2125/01/$ – see front matter 
PII: S0165-2125(01)00091-9

in free-space [4,5] and on an infinite dielectric slab [6], slits in a finite ground plane [7]. Recently, the method has been extended to semi-infinite planar dipole arrays [8,9], and to right-angle sectoral planar phased arrays of dipoles [10].

The asymptotic treatment of each FW aperture distribution on a rectangular array leads to a truncated version of the infinite array FW expansion, plus FW-modulated diffracted contributions from the edges and vertexes of the array. The asymptotic results can be cast in the format of a generalized geometrical theory of diffraction (GTD) ray theory which includes periodicity-induced non-specular reflections as well as multiple periodicity-modulated conical edge diffractions. Since, the FW series and the series of corresponding diffracted fields exhibit excellent convergence properties far enough away from the array plane so that evanescent FWs and diffracted fields are negligible, the resulting representation is found to be more efficient than the direct summation over the spatial contributions from each element of the array. In this paper, the FW-based asymptotic treatment of rectangular AGF is presented and applied to practical array problems.

## 2. Statement of the problem

Let us consider a planar rectangular array comprized of phased elementary electric dipoles of unit current amplitude, located in the $(z_1, z_2)$ plane, as shown in Fig. 1a. Along the $z_1$ and $z_2$ directions, the interelement period is given, respectively, by $d_1$ and $d_2$, the interelement linear phase gradient by $\gamma_1$ and $\gamma_2$, and the number of dipoles by $M$ and $N$. All dipoles are oriented along the unit vector $\hat{u}$ (the caret $\hat{}$ denotes a unit vector) and they are linearly phased.

The AGF $\vec{g}(\vec{r})$ of the $\hat{u}$-directed magnetic vector potential (the arrow $\vec{}$ denotes a vector quantity) at any observation point $\vec{r} = z_1\hat{z}_1 + z_2\hat{z}_2 + y\hat{y}$ is defined by the source-excited harmonic wave equation

$$\nabla^2\vec{g}(\vec{r}) + k^2\vec{g}(\vec{r}) = -\sum_{n=0}^{N-1}\sum_{m=0}^{M-1}\hat{u}\,\mathrm{e}^{-\mathrm{j}(\gamma_1 md_1+\gamma_2 nd_2)}\delta(z_1 - md_1)\delta(z_2 - nd_2) \tag{1}$$

with radiation condition at infinity, and suppressed time dependence $\exp(\mathrm{j}\omega t)$. In (1), $k = \omega/c$ is the free space wavenumber, $c$ is the wave speed in the ambient medium, and $\delta$ the Dirac delta function. The solution is obtained by finite summation over the individual dipole vector potentials

$$\vec{g}(\vec{r}) = \hat{u}g(\vec{r}) = \hat{u}\sum_{m=0}^{M-1}\sum_{n=0}^{N-1} g_0(\vec{r}; md_1, nd_2)\,\mathrm{e}^{-\mathrm{j}(\gamma_1 md_1+\gamma_2 nd_2)}, \tag{2}$$

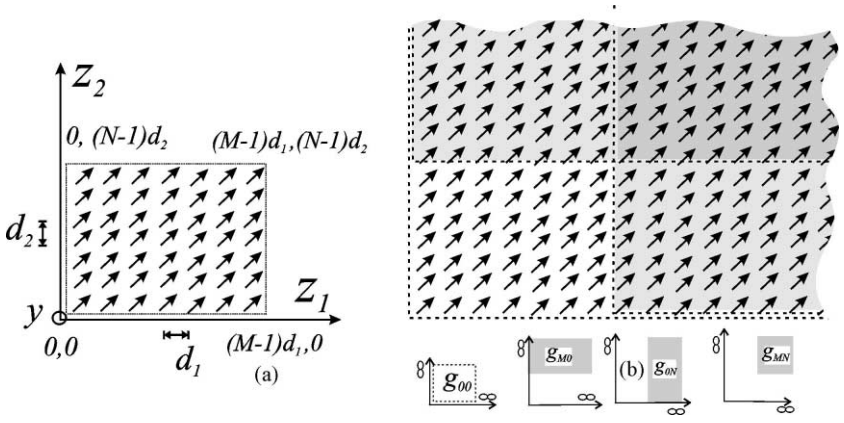


Fig. 1. Actual and auxiliary array geometries: (a) actual rectangular array, (b) auxiliary infinite sectoral arrays.

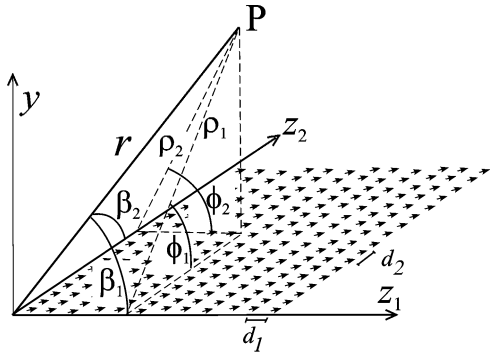


Fig. 2. (a) Geometry of planar sectoral array of parallel dipoles oriented along a direction $\hat{u}$. $d_1$ and $d_2$ are the interelement spatial periods along $z_1$ and $z_2$, respectively.

where

$$g_0(\vec{r}; z_1', z_2') = \frac{\exp(-\mathrm{j}kR(z_1', z_2'))}{4\pi R(z_1' z_2')} \tag{3}$$

is the free-space scalar Green's function with $R(z_1', z_2') = |\vec{r} - (z_1'\hat{z}_1 + z_2'\hat{z}_2)|$. Due to the slow spatial decay of $g(\vec{r}; md_1, nd_2)$, the sum in (2) is slowly convergent for large $M$ and $N$. Collective restructuring into a sum of truncated FWs alleviates this difficulty. Before doing this, (3) is decomposed into four terms,

$$g(\vec{r}) = g_{0,0}(\vec{r}) - g_{M,0}(\vec{r}) - g_{0,N}(\vec{r}) + g_{M,N}(\vec{r}), \tag{4}$$

where

$$g_{\mu,\nu}(\vec{r}) = \sum_{m=\mu}^{\infty}\sum_{n=\nu}^{\infty} g_0(\vec{r}; md_1, nd_2)\, \mathrm{e}^{-\mathrm{j}(\gamma_1 md_1 + \gamma_2 nd_2)} \tag{5}$$

with $(\mu, \nu) = (0, 0), (M, 0), (0, N), (M, N)$, respectively. Each term in (4) represents the AGF of a plane infinite sectoral array with vertex at $(0, 0), (Md_1, 0), (0, Nd_2), (Md_1, Nd_2)$, respectively, as shown in Fig. 1b. Note that each sectoral AGF contribution $g_{\mu,\nu}$ with $(\mu, \nu) \neq (0, 0)$ can be expressed in terms of $g_{0,0}$ as

$$g_{\mu,\nu}(\vec{r}) = g_{0,0}(\vec{r} - \mu d_1\hat{z}_1 - \nu d_2\hat{z}_2)\, \mathrm{e}^{-\mathrm{j}(\gamma_1 \mu d_1 + \gamma_2 \nu d_2)} \tag{6}$$

so that we need treat only the contribution $g_{0,0}(\vec{r})$ of the sectoral array with vertex at the origin.

The geometrical quantities associated with this sectoral array are defined in Fig. 2. Note that this array can be regarded as the superposition, in the $z_2$-direction, of $z_1$-directed semi-infinite line arrays, or vice versa. The truncating line arrays along the $z_1$ and $z_2$ axes give rise to the edge and vertex diffractions of the sectoral array.

## 3. Analytic methods for AGF

The mathematical basis for restructuring the spatial series in (5) into a more rapidly converging series is based on the Poisson sum formula [11]. Let us first consider the infinite bilateral version of this formula, which is pertinent to the infinite array case (Section 3.1), and then proceed to the truncated version for the sectoral array (Section 3.2).

### 3.1. Bilateral Poisson summation

The AGF for the infinite array is obtained by implementing the summation in (2) and (3) from $-\infty$ to $+\infty$ for both indexes $n$ and $m$. It is well known that the AGF can in this case be restructured into discrete global plane wave spectra that obey the Floquet dispersion relation. This is achieved directly using the bilateral Poisson summation formula, which expresses any infinite series of terms indexed by integers $(n, m)$ as an infinite $(q, p)$-indexed series of the relevant Fourier transforms (FTs),

$$g_\infty(\vec{r}) = \sum_{m,n=-\infty}^{\infty} g_0(\vec{r}; md_1, nd_2)\, \mathrm{e}^{-\mathrm{j}(\gamma_1 md_1 + \gamma_2 nd_2)} = \frac{1}{d_1 d_2} \sum_{p,q=-\infty}^{\infty} G(k_{z1,q}, k_{z2,p}), \tag{7}$$

where $G(k_{z1,q}, k_{z2,p})$ is the bilateral FT of $g(\vec{r}; z_1', z_2')$ [12]

$$G(k_{z1}, k_{z2}) = \int_{-\infty}^{\infty}\int_{-\infty}^{\infty} g_0(\vec{r}; z_1', z_2')\, \mathrm{e}^{\mathrm{j}(k_{z1}z_1' + k_{z2}z_2')}\, \mathrm{d}z_1\, \mathrm{d}z_2, \tag{8}$$

sampled at the spectral points

$$k_{z1,q} = \gamma_1 + \frac{2\pi q}{d_1}, \quad q = 0, \pm 1, \pm 2, \ldots, \tag{9}$$

$$k_{z2,p} = \gamma_2 + \frac{2\pi p}{d_2}, \quad p = 0, \pm 1, \pm 2, \ldots. \tag{10}$$

Eqs. (9) and (10) define the FW wavenumbers (i.e., the FW dispersion relations) along the $z_1$ and $z_2$ directions, respectively.

The bilateral FT in (8) can be evaluated in the closed form [13, p. 119]

$$G(k_{z1}, k_{z2}) = \frac{\mathrm{e}^{-\mathrm{j}\vec{k}\cdot\vec{r}}}{k_y}, \qquad \vec{k} = k_{z1}\hat{z}_1 + k_{z2}\hat{z}_2 \pm k_y\hat{y}, \quad k_y = \sqrt{k^2 - k_{z1}^2 - k_{z2}^2}, \tag{11}$$

where the upper and lower signs apply to $y > 0$ and $y < 0$, respectively. Because of the symmetry, we shall deal only with $y > 0$ from here on. Introducing (11) in (7) leads to

$$g_\infty(\vec{r}) = \sum_{p,q=-\infty}^{\infty} g_{pq}^{\mathrm{FW}}(\vec{r}), \qquad g_{pq}^{\mathrm{FW}}(\vec{r}) = \frac{1}{d_1 d_2} \frac{\mathrm{e}^{-\mathrm{j}\vec{k}_{pq}^{\mathrm{FW}}\cdot\vec{r}}}{k_{ypq}}, \tag{12}$$

where $g_{pq}^{\mathrm{FW}}(\vec{r})$ are the FWs for the infinite array and

$$\vec{k}_{pq}^{\mathrm{FW}} = k_{z1,q}\hat{z}_1 + k_{z2,p}\hat{z}_2 + k_{ypq}\hat{y}, \qquad k_{ypq} = \sqrt{k^2 - k_{z1,q}^2 - k_{z2,p}^2} \tag{13}$$

is the FW propagation vector. For a propagating FW (PFW), $\vec{k}_{pq}^{\mathrm{PFW}}$ is real and identifies the radiation (ray) direction of the $pq$th PFW ($\mathrm{PFW}_{pq}$). For an evanescent FW (EFW), the $y$ component $k_{ypq}$ of $\vec{k}_{pq}^{\mathrm{EFW}}$ (perpendicular to the array) is positive imaginary. The EFWs propagate along the array plane with phase propagation vector $\mathcal{R}e(\vec{k}_{pq}^{\mathrm{EFW}})$, maintaining a phase speed less than the speed of light ($|\mathcal{R}e(\vec{k}_{pq}^{\mathrm{EFW}})| > k$), and exhibiting exponential decay along $|y|$. Consequently, the series in (12) is very rapidly convergent when the observation point is far enough away from the array surface.

### 3.2. Truncated Poisson summation

The truncated Poisson sum [11],

$$\sum_{m=0}^{\infty} f(md) = \frac{1}{2} f(0) + \frac{1}{d} \sum_{q=-\infty}^{\infty} \int_0^{\infty} f(z)\, \mathrm{e}^{\mathrm{j}(2\pi q/d)z}\, \mathrm{d}z, \tag{14}$$

transforms a truncated series of samples $f(md)$ into a superposition of $q$-indexed sampled truncated FTs. The extension of this formula to two variable functions is the mathematical basis for treating the sectoral AGF defined in (4). This extension can be accomplished by sequentially applying the one-dimensional truncated Poisson sum in (14); more analytical details are given in the technical report [14]. This leads to

$$g_{0,0}(\vec{r}) = \frac{1}{d_1 d_2} \sum_{p,q=-\infty}^{\infty} \tilde{\tilde{G}}(k_{z1q}, k_{z2p}) + \frac{1}{2d_1} \sum_{q=-\infty}^{\infty} \tilde{G}_2(k_{z1q}) + \frac{1}{2d_2} \sum_{p=-\infty}^{\infty} \tilde{G}_2(k_{z2p}) + \frac{1}{4}\, g(\vec{r}; 0, 0), \tag{15}$$

where $\tilde{\tilde{G}}$ is the two-dimensional truncated FT

$$\tilde{\tilde{G}}(k_{z1}, k_{z2}) = \int_0^{\infty} \int_0^{\infty} g_0(\vec{r}; z_1', z_2')\, \mathrm{e}^{\mathrm{j}k_{z1}z_1'}\, \mathrm{e}^{\mathrm{j}k_{z2}z_2'}\, \mathrm{d}z_1'\, \mathrm{d}z_2' \tag{16}$$

and $\tilde{G}_1$, $\tilde{G}_2$, are truncated FTs of $g(\vec{r}; z_1', z_2')$ with respect to one spatial variable, the other variable being fixed at the origin

$$\tilde{G}_1(k_{z1}) = \int_0^{\infty} g_0(\vec{r}; z_1', 0)\, \mathrm{e}^{\mathrm{j}k_{z1}z_1'}\, \mathrm{d}z_1, \tag{17a}$$

$$\tilde{G}_2(k_{z2}) = \int_0^{\infty} g_0(\vec{r}; 0, z_2')\, \mathrm{e}^{\mathrm{j}k_{z2}z_2'}\, \mathrm{d}z_2'. \tag{17b}$$

In (15), the AGF is represented by four terms. The first term expresses the radiation due to the $pq$-indexed FW planar equivalent current distributions on the sectoral array. The second term is one-half of the radiation of the truncated line array of dipoles located along edge 1, rearranged equivalently in terms of truncated FW-modulated $q$-indexed smooth line sources. The field radiated by these line sources can be interpreted asymptotically as part of the diffracted field induced by all $q$-indexed FW truncated at edge 1. The factor $\frac{1}{2}$ arises from the truncated Poisson formula (14) when the sectoral array is viewed as a $z_2$-truncated collection of semi-infinite line arrays along $z_1$ (see Fig. 2). The third term can be interpreted analogously by interchanging $z_1$ and $z_2$. The last contribution is the radiation from the dipole located at the sectoral array tip, weighted by $\frac{1}{4}$ because of the sequential multiplication of factors $\frac{1}{2}$ pertaining to the two intersecting edge line arrays. This latter contribution is part of the FW-induced vertex-diffracted wave.

### 3.3. Non-uniform asymptotics and shadow boundaries

Integrals (16), (17a) and (17b) can be evaluated asymptotically in terms of saddle point (SP) and end-point contributions on the truncated integration domain. These various critical points are summarized in Table 1. Considered hereafter are only *real critical points* in the space domain, which are associated with propagating FWs, propagating edge diffracted waves, and vertex diffraction. A more complete treatment of EFW and edge diffracted wave contributions may be found in [8,9]. By using (3) in (15)–(17a) and (17b), the phase function in the $\tilde{\tilde{G}}_{pq}$ integrand (see (16)) is $f(z_1', z_2') = -kR(z_1', z_2') + z_1' k_{z1,q} + z_2' k_{z2,q}$ and those of $\tilde{G}_q$ and $\tilde{G}_p$ (see (17a) and (17b)) are $f(z_1', 0)$ and $f(0, z_2')$, respectively.

Table 1
Critical points of the space-domain integrals[a]

| Integral | Critical points $f(z_1', z_2') = -kR(z_1', z_2') + z_1' k_{z1,q} + z_2' k_{z2,q}$ | Analytic expressions |
|---|---|---|
| $\tilde{G}_q(k_{z1q})$ | SP: $\frac{\partial}{\partial z_1'} f(z_1', 0) = 0 \rightarrow z_1' = z_{1q} \rightarrow$ edge-1 diffracted ray | $z_{1q} = z_1 - \rho_1, \frac{k_{z1,q}}{k_{\rho 1,q}} = z_1 - \rho_1 \cot\beta_{1,q}$ |
| | EP: $z_1' = 0 \rightarrow$ vertex-diffracted ray | $k_{p1q} = \sqrt{k^2 - k_{z1q}^2}$ |
| $\tilde{G}_p(k_{z2p})$ | SP: $\frac{\partial}{\partial z_2'} f(0, z_2') = 0 \rightarrow z_2' = z_{2p} \rightarrow$ edge-2 diffracted ray | $z_{2p} = z_2 - \rho_2, \frac{k_{z2,p}}{k_{p2,p}} = z_2 - \rho_2 \cot\beta_{2,p}$ |
| | EP: $z_2' = 0 \rightarrow$ vertex-diffracted ray | $k_{\rho 2p} = \sqrt{k^2 - k_{z2p}^2}$ |
| $\tilde{\tilde{G}}_{pq}(k_{z1q}, k_{z2p})$ | 2D-SP: $\nabla f(z_1', z_2') = 0 \rightarrow (z_1', z_2') = (z_{1pq}, z_{2pq}) \rightarrow$ FW | $z_{1pq} = z_1 + y\frac{k_{z1,q}}{k_{ypq}} = z_1 + y\frac{\cot\beta_{1,q}}{\sin\phi_{1,pq}}$ |
| | EP–SP: $(z_1', z_2') = (0, z_{2p})$ edge-2 diffracted ray | $z_{2pq} = z_2 + y\frac{k_{z2,p}}{k_{ypq}} = z_2 + y\frac{\cot\beta_{2,p}}{\sin\phi_{2,pq}}$ |
| | SP–EP: $(z_1', z_2') = (z_{1q}, 0)$ edge-1 diffracted ray | |
| | EP–EP: $(z_1', z_2') = (0, 0)$ vertex-diffracted ray | |

[a] The first column refers to the space domain integral. Critical points in the space domain are defined in column 2 (SP: saddle point, EP: end-point). Column 3 contains the expressions of the critical points.

The integral which defines $\tilde{\tilde{G}}_{pq}$ is dominated by the 2D-SP contribution $(z_1', z_2') = (z_{1pq}, z_{2pq})$ satisfying $\nabla f(z_1', z_2') = 0$, whose explicit expression is given in Table 1. The phase at the SP $f(z_{1pq}, z_{2pq})$ can be rewritten as $\vec{k}_{pq}^{\,\mathrm{FW}} \cdot \vec{r}$ (Table 2) with the FW wavenumber vector $\vec{k}_{pq}^{\,\mathrm{FW}}$ given in (13). The asymptotic $pq$th contributions from $(z_{1pq}, z_{2pq})$ are FW-rays emanating from the array surface at points $(z_{1pq}, z_{2pq})$, which are generalizations of the conventional geometrical optic rays (see Fig. 3a). Only propagating FWs imply real values of $(z_{1pq}, z_{2pq})$. These asymptotic contributions exist only when $z_{1pq} > 0$ and $z_{2pq} > 0$, i.e., when they lie within the truncated integration domain. This leads to a truncated version of the FW series in (12)

$$g^{\mathrm{FW}}(\vec{r}) = \sum_{p,q} g_{pq}^{\mathrm{FW}}(\vec{r}) U_{pq}^{\mathrm{FW},1} U_{pq}^{\mathrm{FW},2}, \qquad U_{pq}^{\mathrm{FW},1} = U(z_{2pq}), \quad U_{pq}^{\mathrm{FW},2} = U(z_{1pq}), \tag{18}$$

where $U(z)$ is the Heaviside unit step function: $U(z) = 1$ for $z > 0$ and $U(z) = 0$ for $z < 0$.

The truncation functions can be rewritten in terms of angular quantities as

$$U_{pq}^{\mathrm{FW},1} = U(\phi_{1,pq}^{\mathrm{SB}} - \phi_1), \qquad U_{pq}^{\mathrm{FW},2} = U(\phi_{2,pq}^{\mathrm{SB}} - \phi_2), \tag{19}$$

Table 2
Wavevectors and shadow boundaries[a]

| Ray contribution | Wavevectors | SB |
|---|---|---|
| FW-$pq$ ray | $f(z_{sq}, z_{sp}) = \vec{k}_{pq}^{\,\mathrm{FW}} \cdot \vec{r}, \vec{k}_{pq}^{\,\mathrm{FW}} = k_{z1,q}\hat{z}_1 + k_{z2,p}\hat{z}_2 + k_{ypq}\hat{y}$ | $\phi_1 = \phi_{1,pq}^{\mathrm{SB}}, \phi_2 = \phi_{2,pq}^{\mathrm{SB}}$ |
| Edge-1 diffracted rays | $f(z_{1q}, 0) = \vec{k}_q^{d,1} \cdot \vec{r}, \vec{k}_q^{d,1} = k_{z1,q}\hat{z}_1 + k_{pq,1}\cos\phi_1\hat{z}_2 + k_{pq,1}\sin\phi_1\hat{y}$ | $\beta_1 = \beta_{1,q}^{\mathrm{SB}} \equiv \beta_{1,q}$ |
| Edge-2 diffracted rays | $f(0, z_{2p}) = \vec{k}_p^{d,2} \cdot \vec{r}, \vec{k}_p^{d,2} = k_{z2,p}\hat{z}_2 + k_{\rho p,2}\cos\phi_2\hat{z}_1 + k_{\rho p,2}\sin\phi_2\hat{y}$ | $\beta_2 = \beta_{2,p}^{\mathrm{SB}} \equiv \beta_{2,p}$ |
| Vertex-diffracted ray | $f(0,0) = \vec{k}^v \cdot \vec{r}; \vec{k}^v = \frac{k\vec{r}}{\lvert\vec{r}\rvert}$ | |

[a] The second column contains the expressions of the wavevectors associated with the various ray contributions. The third column contains the analytical expressions of shadow boundary planes of FW and shadow boundary cones of edge diffracted rays ($\beta_{1,q} = \cos^{-1}(k_{z1,q}/k)$; $\beta_{2,p} = \cos^{-1}(k_{z2,p}/k)$).

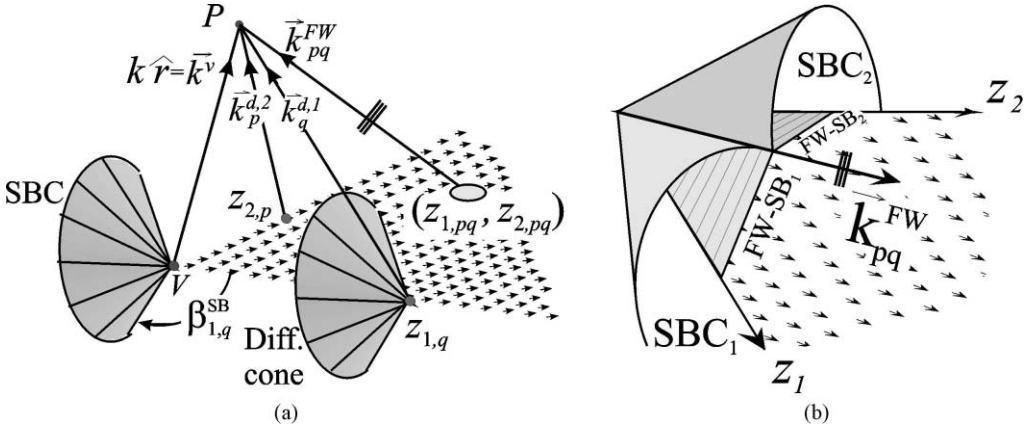


Fig. 3. (a) Ray description of the field radiated by the sectoral array of dipoles. The diffraction cone of the propagating $z_1$-edge diffracted ray originates at the $q$-dependent point $Q_{1,q}$ on edge 1. The SBC that truncates the domain of existence has the same aperture angle $\beta_{1,q}$ as the diffraction cone and it is centered at the vertex. (b) Geometry of the shadow boundaries (SB). The FW–SB planes truncate the domain of existence of an FW with index $pq$. The truncated $FW_{pq}$ exists under the "roof" formed by the intersection of the two FW–SB. The diffracted rays from edges 1 and 2 are truncated at the shadow boundary cones (SBC) with axes along edges 1 and 2. These two SBCs intersect along the intersection line of the two FW–SBs. This intersection line coincides with the propagation vector $\vec{k}_{pq}$ of the $pq$-FW.

where $\phi_i$ is the transverse-to-$z_i$ observation angle (see Fig. 2). The domain of existence of the $FW_{pq}$ (the $FW_{pq}$-illuminated region) is thereby truncated at the shadow boundary planes (SB) $\phi_1 = \phi_{1,pq}^{SB}$, where for PFWs, $\phi_{1,pq}^{SB} \equiv \phi_{1,pq} = \cos^{-1}(k_{z2,p}/k_{\rho 1,q})$ and $k_{\rho 1,q} = \sqrt{k^2 - k_{z1,q}^2}$ (with analogous definition for $\phi_{2,pq}^{SB}$).

The asymptotic treatment of (16) also includes the contributions from the 1D-SP at the boundary of the spatial integration domain; these are given by $z_{1q}$ and $z_{2p}$ shown in Table 1, which satisfy the equations $\partial/\partial z_1' f(z_1', 0) = 0$ and $\partial/\partial z_2' f(0, z_2') = 0$, respectively. The corresponding ray contributions are FW-induced edge diffracted rays from edges 1 and 2, respectively. The same critical points and ray interpretation of the relevant asymptotic contributions pertain to the line integrals in (17a) and (17b) for edges 1 and 2, respectively. The phase at the SP can be expressed as $f(z_{1q}, 0) = \vec{k}_q^{d,1} \cdot \vec{r}$, where $\vec{k}_q^{d,1}$ (defined in Table 2) is the vector wavenumber of the $q$-indexed edge diffracted ray. For $|k_{z1,q}| < k$ (see Fig. 3a) this ray reaches the observer along a diffraction cone with angle $\beta_{1,q} = \cos^{-1}(k_{z1,q}/k)$, emerging from the diffraction points $z_{1q}$; $|k_{z1,q}| > k$ implies complex values of $z_{1q}$ which correspond to evanescent diffracted waves and are not treated here. Edge-2 diffracted rays are analogously obtained from the $z_2$-SP in the integrands of (16) and (17b). The above rays are FW-modulated generalizations of the smooth-edge diffracted rays in conventional GTD.

The diffracted ray contributions from edge 1 are the same as those for a semi-infinite array of dipoles [8,9] with the edge aligned along the corresponding edge of the sectoral array, but they abruptly emerge or disappear when, for a moving observer, $z_{1q}$ crosses the vertex $z_1 = 0$. Thus, edge 1-diffracted rays are multiplied by the truncation function

$$U_q^{d,1} \equiv U(z_{1,q}) = U(\beta_{1,q}^{SB} - \beta_1), \tag{20}$$

expressed in terms of the conical angles $\beta_{1,q}^{SB} \equiv \beta_{1,q} = \cos^{-1}(k_{z1,q}/k)$ and indicating that the diffracted field is confined by the shadow boundary cone $SBC_{1,q}$ (Fig. 3a and b). The $SBC_{1,q}$, centered at the vertex, has the same aperture as the diffraction cone (19). Analogous considerations apply to the $p$-indexed, $q$-independent $z_2$-edge diffracted rays, whose domain of existence is confined by $U_p^{d,2} \equiv U(z_{2,p}) = U(\beta_{2,p}^{SB} - \beta_2)$ with $\beta_{2,p}^{SB} \equiv \beta_{2,p} = \cos^{-1}(k_{z2,p}/k)$.

The vertex-diffracted ray contributions arise from the 2D end-point (EP) at $(z_1', z_2') = (0, 0)$ of (16) and from the 1D EPs at $z_1' = 0$ and $z_2' = 0$ of (17a) and (17b), respectively (Table 1). The phase $f(0, 0)$ at these EPs can be

written as $\vec{k}^v \cdot \vec{r}$, where $\vec{k}^v \equiv k\vec{r}/r = k\hat{r}$ (see Table 2) is the wave propagation vector of the vertex-diffracted ray centered at the vertex. This ray also comprises the contribution $\frac{1}{4}g(\vec{r}; 0, 0)$.

Grouping all the asymptotic terms pertaining to the various wave species (i.e., FWs, edge diffracted waves and vertex wave) together, the sectoral AGF is expressed as

$$g_{0,0}(\vec{r}) \sim g^{\mathrm{FW}}(\vec{r}) + \sum_q U_q^{d,1} g_q^{d,1}(\vec{r}) + \sum_p U_p^{d,2} g_p^{d,2}(\vec{r}) + g^v(\vec{r}) \tag{21}$$

with $g^{\mathrm{FW}}(\vec{r})$ are the truncated FWs defined in (18) and $g_q^{d,1}$ ($g_p^{d,2}$) contain the $q$-indexed ($p$-indexed) edge-diffracted contributions from edge 1 (edge 2) due to the integrals (16), (17a) and (17b), and $g^v(\vec{r})$ contains all vertex contributions, including $\frac{1}{4}g(\vec{r}; 0, 0)$.

### *3.4. Spectral domain version of the truncated Poisson sum*

In the vicinity of the shadow boundary of any FW or edge-diffracted wave species, non-uniform asymptotics generally becomes inapplicable. Uniform asymptotic methods must be invoked there in order to ensure smooth compensation of the abrupt emergence or disappearance of any particular wave species across its SB. The (FW–SB)-(edge-diffracted) compensation mechanism away from the vertex is the same as that from a semi-infinite array of dipoles with its edge aligned along the sectoral array edge [8,9]. Near the vertex, the two FW–SB transitions interact with the vertex-induced SBC transitions, due to the truncation of the corresponding edge diffracted fields (Fig. 3a and b). The confluence of these four SB transitions near the vertex defines the asymptotics pertaining to vertex diffraction [10].

The high-frequency formulation which uniformly describes the sectoral AGF in the various transition regions will be developed by applying the truncated Poisson summation formula (15) in the rectilinear spectral domain $(k_{z1}, k_{z2})$. To this end, we write the truncated FTs in (17a) and (17b) in terms of a bilateral FT $G(k_{z1}, k_{z2})$ in (8) by using a spectral convolution of $G(k_{z1}, k_{z2})$ with the FT, $-1/k_{z1}k_{z2}$ of the 2D unit step function $U(z_1)U(z_2)$,

$$\tilde{\tilde{G}}(k_{z1,q}, k_{z2,p}) = \int_{-\infty}^{\infty}\int_{-\infty}^{\infty} \frac{-G(k_{z1}, k_{z2})}{(k_{z1,q} - k_{z1})(k_{z2,p} - k_{z2})}\, \mathrm{d}k_{z1}\, \mathrm{d}k_{z2}. \tag{22}$$

The same spectral convolution may be applied to the one-dimensional integrations in (17a) and (17b),

$$\tilde{G}_1(k_{z1,q}) = \int_{-\infty}^{\infty} \frac{G_1(k_{z1}, z_2' = 0)}{\mathrm{j}(k_{z1,q} - k_{z1})}\, \mathrm{d}k_{z1}, \tag{23a}$$

$$\tilde{G}_2(k_{z2,p}) = \int_{-\infty}^{\infty} \frac{G_2(k_{z2}, z_1' = 0)}{\mathrm{j}(k_{z2,p} - k_{z2})}\, \mathrm{d}k_{z2}, \tag{23b}$$

where $G_1(k_{z1}, z_2' = 0)$ and $G_2(k_{z2}, z_1' = 0)$ are the bilateral FTs of $g_0(\vec{r}; z_1', 0)$ and $g_0(\vec{r}; 0, z_2')$, respectively. Since the unit step function $U$ is represented as a residue from a clockwise spectral integration around the pole $1/k_{zi}$, the integration contours in (22), (23a) and (23b) are indented clockwise around the poles $k_{z1,q}$ and $k_{z2,p}$.

The functions $G_1(k_{z1}, z_2' = 0)$ and $G_2(k_{z2}, z_1' = 0)$ can be represented in terms of an inverse FT as $G_1(k_{z1}, z_2' = 0) = \int_{-\infty}^{\infty} G(k_{z1}, k_{z2})\, \mathrm{d}k_{z2}$, and $G_2(k_{z2}, z_1' = 0) = \int_{-\infty}^{\infty} G(k_{z1}, k_{z2})\, \mathrm{d}k_{z1}$, thus leading to the double spectral integral representations

$$\tilde{G}_1(k_{z1,q}) = \int_{-\infty}^{\infty}\int_{-\infty}^{\infty} \frac{G(k_{z1}, k_{z2})}{\mathrm{j}(k_{z1,q} - k_{z1})}\, \mathrm{d}k_{z1}\, \mathrm{d}k_{z2}, \tag{24a}$$

$$\tilde{G}_2(k_{z2,p}) = \int_{-\infty}^{\infty}\int_{-\infty}^{\infty} \frac{G(k_{z1}, k_{z2},)}{\mathrm{j}(k_{z2,p} - k_{z2})}\, \mathrm{d}k_{z1}\, \mathrm{d}k_{z2}. \tag{24b}$$

Analogously, using the inverse FT of (8) evaluated at $(z_1', z_2') = (0, 0)$ yields

$$\frac{1}{4}g_0(\vec{r};0,0) = \frac{1}{4}\frac{1}{(2\pi)^2}\int_{-\infty}^{\infty}\int_{-\infty}^{\infty} G(k_{z1},k_{z2})\,\mathrm{d}k_{z1}\,\mathrm{d}k_{z2}. \tag{25}$$

After insertion of (22), (24a), (24b) and (25) into (15), interchange of the order of summation and integration, and symmetric regrouping of the $q$-indexed and $p$-indexed series, one obtains

$$g_{0,0}(\vec{r}) = \int_{-\infty}^{\infty}\int_{-\infty}^{\infty} G(k_{z1},k_{z2})\left(\frac{1}{2}+\sum_{q=-\infty}^{\infty}\frac{1}{\mathrm{j}d_1(k_{z1,q}-k_{z1})}\right)\left(\frac{1}{2}+\sum_{p=-\infty}^{\infty}\frac{1}{\mathrm{j}d_2(k_{z2,p}-k_{z2})}\right)\mathrm{d}k_{z1}\,\mathrm{d}k_{z2}. \tag{26}$$

Using the identity

$$\frac{1}{2}+\frac{1}{\mathrm{j}d_i}\sum_{i=-\infty}^{\infty}\frac{1}{k_{zi,\xi}-k_{zi}} = \frac{1}{2}+\frac{1}{2\mathrm{j}}\cot\left[\frac{1}{2}d_i(\gamma_i-k_{zi})\right] = \frac{1}{1-\mathrm{e}^{\mathrm{j}d_i(k_{zi}-\gamma_i)}} = B_i(k_{zi}), \quad i=1,2 \tag{27}$$

along with (11) leads to the compact form

$$g_{0,0}(\vec{r}) = \frac{1}{8\pi^2\mathrm{j}}\int_{-\infty}^{\infty}\int_{-\infty}^{\infty}\frac{1}{k_y}B_1(k_{z1})B_2(k_{z2})\,\mathrm{e}^{-\mathrm{j}\vec{k}\cdot\vec{r}}\,\mathrm{d}k_{z1}\,\mathrm{d}k_{z2}, \tag{28}$$

where $k_y$ is defined in Eq. (11). The representation (28) is the same as that in [10], which has been derived directly from the space domain summation in (5).

### 3.5. Uniform asymptotic evaluation of the AGF

The high-frequency behavior of the exact solution given by the spectral double integral (28) is parameterized by the critical points in the integrand which also govern the strategies for the uniform asymptotic approximations. The critical points are defined and described in Table 3; $k_{z1}$-poles at $k_{z1,q}$ (due to $B_1$) and $k_{z2}$-poles at $k_{z2,p}$ (due to $B_2$); first-order $(k_{z1},k_{z2})$-SP $(\bar{k}_{z1s},\bar{k}_{z2s})$, due to the phase $k\cdot\vec{r}$. Asymptotic evaluation of (28) parameterizes the sectoral AGF behavior in terms of the phenomenologies of two semi-infinite arrays (SIAs) with edge aligned along the two edges of the sector. As formulated in [10], these phenomenologies are extracted from the spectral integrals in (24a) and (24b) by sequential deformation of the two integration contours into local steepest descent paths (SDPs) through SPs. This operation is complicated by the fact that the SPs and the SDPs must be tracked in two complex planes $(k_{z1},k_{z2})$ simultaneously. Remaining cognizant of the constituent SIA solutions, the problem is addressed by deforming the original integration path locally into the complex $k_{z2}$-SDP along the 45° line through the $k_{z1}$-dependent SP $k_{z2s}(k_{z1}) = \sqrt{k^2-k_{z1}^2}\cos\phi_1$ (see Table 3). This leads to

$$g_{0,0}(\vec{r}) = \bar{g}_{0,0}(\vec{r}) + I_2(\vec{r}), \qquad I_2(\vec{r}) = \int_{-\infty}^{\infty}\sum_p \mathfrak{B}_{2p}(k_{z1})\,\mathrm{e}^{-\mathrm{j}k\mathfrak{I}_{2p}(k_{z1})}\,\mathrm{d}k_{z1}, \tag{29}$$

where $\bar{g}_{0,0}$ is the same as in (28), but along the deformed local SDP in the $k_{z2}$ variable (see Table 3), and $I_2(\vec{r})$ arises from the $k_{z1}$-dependent residues at the poles $k_{z2,p}$ intercepted during the deformation. In (29), $\mathfrak{B}_{2p}(k_{z1}) = -B_1(k_{z1})[4\pi\mathrm{j}d_1k_{y2,p}]^{-1}U[k_{z2s}(k_{z1})-k_{z2,p}]$, with $k_{y2,p} = \sqrt{k^2-k_{z1}^2-k_{z2,p}^2}$, contains poles at $k_{z1}=k_{z1,q}$ due to $B_1(k_{z1})$ in (27) and incorporates a spectral truncation function; the phase $\mathfrak{I}_{2p}(k_{z1})$ in the integrand is defined in

Table 3
Critical points of the spectral domain integrals[a]

| Integrals and spectral phases | Critical points $(\bar{k}_{z1s}, \bar{k}_{z2s}) = (k\cos\beta_1, k\cos\beta_2)$ | Analytic expressions |
|---|---|---|
| $g_{0,0}(\vec{r}) \rightarrow$ (28) | 2D-SP: $\bar{\nabla}\mathfrak{I}(k_{z1}, k_{z2}) = 0$, $(\bar{k}_{z1s}, \bar{k}_{z2s}) \Uparrow$ vertex ray | $\mathfrak{I}(\bar{k}_{z1s}, \bar{k}_{z2s}) = \vec{k}^v \cdot \vec{r} = kr$ |
| $\mathfrak{I}(k_{z1}, k_{z2}) \equiv \vec{k} \cdot \vec{r}$; $\vec{k} = k_{z1}\hat{z}_1 + k_{z2}\hat{z}_2 + k_y y$ | Poles: $(k_{z1}, k_{z2}) = (k_{z1,q}, k_{z2,p}) \rightarrow$ truncated FW | $\mathfrak{I}(k_{z1,q}, k_{z2,p}) = \vec{k}_{pq}^{\,\mathrm{FW}} \cdot \vec{r}$ |
| | 1D-SP: $\dfrac{\partial}{\partial k_{z2}}\mathfrak{I}(k_{z1}, k_{z2}) = 0$; $k_{z2s}(k_{z1})$ (see Fig. a) | $k_{z2s}(k_{z1}) = \sqrt{k^2 - k_{z1}^2}\cos\phi_1$ |
| | 1D-SP: $\dfrac{\partial}{\partial k_{z1}}\mathfrak{I}(k_{z1}, k_{z2}) = 0$; $k_{z1s}(k_{z2})$ (see Fig. b) | $k_{z1s}(k_{z2}) = \sqrt{k^2 - k_{z2}^2}\cos\phi_2$ |
| $g_{00} = \bar{\bar{g}}_{00} + I_{1,\mathrm{SDP}} + I_{2,\mathrm{SDP}} + g^{\mathrm{FW}}$ | | |
| $I_{1,\mathrm{SDP}}(\vec{r}) \rightarrow$ (31) $\rightarrow$ edge-1 diffracted rays | SP: $\dfrac{\partial}{\partial k_{z2}}\mathfrak{I}_{1q}(k_{z2}) = 0$; $k_{s2,q}$ | $k_{s2,q} = \sqrt{k^2 - k_{z1,q}^2}\cos\phi_1$ |
| $\mathfrak{I}_{1q}(k_{z2}) = k_{z2}z_2 + k_{z1,q}z_1 + y\sqrt{k^2 - k_{z2}^2 - k_{z1,q}^2}$ | Poles: $k_{z2} = k_{z2,p} \rightarrow$ SB1 transition region | $\mathfrak{I}_{1q}(k_{s2,q}) = \vec{k}_q^{\,d,1} \cdot \vec{r}$ |
| $I_{2,\mathrm{SDP}}(\vec{r}) \rightarrow$ (30) $\rightarrow$ edge-2 diffracted rays | SP: $\dfrac{\partial}{\partial k_{z1}}\mathfrak{I}_{2p}(k_{z1}) = 0$; $k_{s1,p}$ | $k_{s1,p} = \sqrt{k^2 - k_{z2,p}^2}\cos\phi_2$ |
| $\mathfrak{I}_{2p}(k_{z1}) = k_{z1}z_1 + k_{z2,p}z_2 + y\sqrt{k^2 - k_{z1}^2 - k_{z2,p}^2}$ | Poles: $k_{z1} = k_{z1,q} \rightarrow$ SB2 transition region | $\mathfrak{I}_{2p}(k_{s1,p}) = \vec{k}_p^{\,d,2} \cdot \vec{r}$ |

[a] The first column refers to the spectral integrals and defines relevant spectral quantities. Critical spectral points are defined in column 2. Column 3 contains expressions for the phase function and other spectral quantities evaluated at the critical points. $\bar{\nabla}$ is the gradient in the spectral domain.

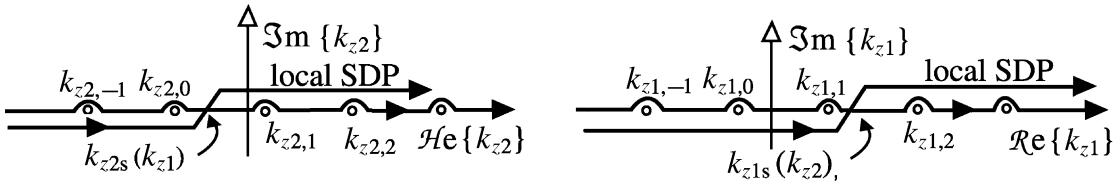


Table 3. The $k_{z1}$ real-axis integration path of $I_2(\vec{r})$ is then deformed into the local SDP through the SP of $\mathfrak{I}_{2p}(k_{z1})$, and the residues at the poles intercepted during this deformation yield the truncated FW series in (18),

$$I_2(\vec{r}) = g^{\mathrm{FW}}(\vec{r}) + I_{2,\mathrm{SDP}}(\vec{r}) \tag{30}$$

where $g^{\mathrm{FW}}(\vec{r})$ denotes the truncated FW sum in (18) with $I_{2,\mathrm{SDP}}$ the same as $I_2$ but with the $k_{z1}$-integration path along the local SDP. A similar contour deformation is now applied to $\bar{g}_{0,0}(\vec{r})$. The $k_{z1}$-integration path is deformed locally into the complex $k_{z1}$-SDP along the 45°-line through the $k_{z2}$-dependent SP $k_{z1s}(k_{z2}) = \sqrt{k^2 - k_{z2}^2}\cos\phi_2$ (see Table 3),

$$\bar{g}_{0,0}(\vec{r}) = \bar{\bar{g}}_{0,0}(\vec{r}) + I_{1,\mathrm{SDP}}(\vec{r}), \qquad I_{1,\mathrm{SDP}}(\vec{r}) = \sum_q \int_{\mathrm{SDP}} \mathfrak{B}_{1q}(k_{z2})\, \mathrm{e}^{-\mathrm{j}k\mathfrak{I}_{1q}(k_{z2})}\, \mathrm{d}k_{z2} \tag{31}$$

with $\bar{\bar{g}}_{0,0}(\vec{r})$ the same as in (28), but along local SDP integration contours in both variables (see Table 3, and $I_{1,\mathrm{SDP}}(\vec{r})$ arising from the $k_{z1}$-dependent residues at the poles $k_{z2,p}$ intercepted during the deformation. In (31), $\mathfrak{B}_{1q}(k_{z2}) = -B_2(k_{z2})[4\pi\mathrm{j}d_2 k_{y1,q}]^{-1}U[k_{z1s}(k_{z2}) - k_{z1,q}]$, with $k_{y1,q} = \sqrt{k^2 - k_{z2}^2 - k_{z1,q}^2}$, contains poles at $k_{z2} = k_{z2,p}$ due to $B_2(k_{z2})$ defined in (27) and incorporates a spectral truncation function; the phase $\mathfrak{I}_{1q}(k_{z2})$ in the integrand is defined in Table 3.

The two integrals $I_{i,\mathrm{SDP}}(\vec{r})$ with $i = 1$ and 2 in (31) and (30), respectively, represent the diffracted waves from edges 1 and 2. Their critical points are summarized in Table 3, and their uniform asymptotics is carried out by the Van der Waerden (VdW) method for single integrals [15] as described next.

*3.5.1. Truncated edge diffracted waves*

The SDP integrations in (30) are reduced to a canonical form by selectively adding and subtracting in the integrand a "regularizing" function which accommodates relevant configurations of any number of poles with respect to the SP. For the integral in (31)

$$I_{1,\mathrm{SDP}}(\vec{r}) = \int_{\mathrm{SDP}} \sum_q \left( \mathfrak{B}_{1q}(k_{z2}) - \frac{\mathfrak{R}_{1q}}{(k_{z2} - k_{z2p})} \right) \mathrm{e}^{-\mathrm{j}k\mathfrak{I}_{1q}(k_{z2})}\, \mathrm{d}k_{z2} + \Delta I, \tag{32}$$

where $\mathfrak{R}_{1q} = 1/(4\pi d_1 d_2) U[k_{z2s}(k_{z1}) - k_{z2,p}]$ is the residue at the pole $k_{z2pq}$ and $\Delta I$ can be expressed in terms of a Fresnel canonical function. Using first-order Taylor expansion around the SP of the $k_{z2}$-integral in (32) leads to

$$I_{1,\mathrm{SDP}}(\vec{r}) \sim \sum_q g_q^{d,1}(\vec{r}) U(\beta_{1,q}^{\mathrm{SB}} - \beta_1), \tag{33}$$

where $g_q^{d,1}(\vec{r})$ is defined in Table 4. The function $F$ in this table is the transition function of the *uniform theory of diffraction* [16]. This function tends to unity for "large" amplitude of its argument $\delta_{1,pq}$, i.e., for observation points "far" from the SBs. In the same observation range, the quantity $(1 - F)$ is of asymptotic order $(k_{\rho q}\rho)^{-1}$, so that the dominant asymptotic contribution to the diffraction coefficient is $B_2(k_{s2,q}) = B_2(k_{\rho 1,q}\cos\phi_1)$ in Table 4, which characterizes the non-uniform edge diffraction field. Thus, the "large $\delta_{1,pq}$" range connects the transition function $F$ in the second term of $g_q^{d,1}(\vec{r})$ (in Table 4) smoothly with the non-uniform first term in an overlapping region. Note that "large $\delta_{1,pq}$" can be reached: (a) by specifying $\phi_{1,pq} \approx \phi_1$ and/or $\rho_1$ small with large enough $k$, or (b) by specifying $k$ with large enough $(\phi_{1,pq} - \phi_1)$ and/or $\rho_1$. This type of asymptotic "patching" will be utilized repeatedly later on.

Table 4
High-frequency uniform representation of the AGF[a]

| | |
|---|---|
| Total AGF | $g_{0,0}(\vec{r}) \sim \sum_{p,q} U_{pq}^{FW,1} U_{pq}^{FW,2} g_{pq}^{\mathrm{FW}}(\vec{r}) + \sum_q U_q^{d,1} g_q^{d,1}(\vec{r}) + \sum_p U_p^{d,2} g_p^{d,2}(\vec{r}) + g^v(\vec{r})$ |
| Edge-1 diffraction | $g_q^{d,1}(\vec{r}) \sim \dfrac{\mathrm{e}^{-\mathrm{j}\vec{k}_q^{d,1}\cdot\vec{r}}}{2d_1\sqrt{2\pi\mathrm{j}\rho_1 k_{\rho 1,q}}} \left( B_2(k_{s2,q}) + \sum_p \dfrac{(F(\delta_{1,pq}^2) - 1)}{\mathrm{j}d_2(k_{z2,p} - k_{s2,q})} \right)$, $B_2(k_{s2,q}) = [1 - \mathrm{e}^{\mathrm{j}d_2(k_{s2,q} - \gamma_2)}]^{-1}$ |
| Edge-2 diffraction | $g_p^{d,2}(\vec{r}) \sim \dfrac{\mathrm{e}^{-\mathrm{j}\vec{k}_p^{d,2}\cdot\vec{r}}}{2d_2\sqrt{2\pi\mathrm{j}\rho_2 k_{\rho 2,p}}} \left( B_1(k_{s1,p}) + \sum_q \dfrac{(F(\delta_{2,pq}^2) - 1)}{\mathrm{j}d_1(k_{z1,q} - k_{s1,p})} \right)$, $B_1(k_{s1,p}) = [1 - \mathrm{e}^{\mathrm{j}d_1(k_{s1,p} - \gamma_1)}]^{-1}$ |
| Canonical transition function | $F(x) = 2\mathrm{j}\sqrt{x}\,\mathrm{e}^{\mathrm{j}x} \int_{\sqrt{x}}^{\infty} \mathrm{e}^{-\mathrm{j}t^2}\,\mathrm{d}t$; $\begin{pmatrix} \delta_{1,pq} = \sqrt{2k_{\rho 1,q}\rho_1}\sin(\frac{1}{2}(\phi_{1,pq} - \phi_1)) \\ \delta_{2,pq} = \sqrt{2k_{\rho 2,p}\rho_2}\sin(\frac{1}{2}(\phi_{2,pq} - \phi_2)) \end{pmatrix}$ |
| Vertex diffraction | $g^v(\vec{r}) \sim \dfrac{\mathrm{e}^{-\mathrm{j}kr}}{4\pi r} \left( B_1(\bar{k}_{z1s}) B_2(\bar{k}_{z2s}) + \dfrac{B_2(\bar{k}_{z2s})(F(a_q^2) - 1)}{\mathrm{j}d_1(k_{z1,q} - \bar{k}_{z1s})} + \dfrac{B_1(\bar{k}_{z1s})(F(b_p^2) - 1)]}{\mathrm{j}d_2(k_{z2,p} - \bar{k}_{z2s})} + \dfrac{(T(a_q, b_p, w) - F(a_q^2) - F(b_p^2) + 1)}{-d_1 d_2(k_{z1,q} - \bar{k}_{z1s})(k_{z2,p} - \bar{k}_{z2s})} \right)$ |
| Canonical transition function | $T(a_q, b_p, W) = \dfrac{a_q b_p}{\mathrm{j}\pi\sqrt{1 - W^2}} \displaystyle\int_{-\infty}^{\infty}\int_{-\infty}^{\infty} \dfrac{\mathrm{e}^{\mathrm{j}(\xi^2 + 2\omega\xi\eta + \eta^2)}}{(\xi - (a_q/\sqrt{1 - W^2}))(\eta - (b_p/\sqrt{1 - W^2}))}\,\mathrm{d}\xi\,\mathrm{d}\eta a_q$ $= \sqrt{2kr}\sin(\frac{1}{2}(\beta_{1,q} - \beta_1))$, $b_p = \sqrt{2kr}\sin(\frac{1}{2}(\beta_{2,p} - \beta_2))$; $\omega = \cot\beta_1 \cot\beta_2 = \cos\phi_1 \cos\phi_2$ |

[a] Uniform asymptotic constructs and definition of transition functions.

When $|k_{z1,q}| > k$, the resulting diffracted field is evanescent along the $\rho_1$ direction, with exponential decay term $\exp(-|k_{\rho 1,q}|\rho_1)$, since in this case $k_{\rho 1,q} = -\mathrm{j}|k_{\rho 1,q}|$ (see (17a) and (17b)). The radially attenuated diffracted waves are negligible even relatively close to the edge so that the $q$-series of diffracted rays in (14) can be truncated in such a way as to include only propagating diffracted waves (those with $|k_{z1,q}| < k$). This renders the FW formulation substantially more efficient than element-by-element summation. The treatment of the integral $I_{2,\mathrm{SDP}}(\vec{r})$ proceeds like that above with interchange of indexes 1 and 2 and indexes $q$ and $p$; i.e., $I_{2,\mathrm{SDP}}(\vec{r}) \sim \sum_p g_p^{d,2}(\vec{r}) U(\beta_{2,p}^{\mathrm{SB}} - \beta_2)$ with $g_p^{d,2}(\vec{r})$ defined in Table 4.

### 3.5.2. Vertex-diffracted wave

The vertex-diffracted field is given by

$$\overline{\overline{g}}_{0,0}(\vec{r}) = \frac{1}{8\pi^2 \mathrm{j}} \int_{\mathrm{SDP}} \int_{\mathrm{SDP}} \frac{1}{k_y} B_1(k_{z1}) B_2(k_{z2})\, \mathrm{e}^{-\mathrm{j}\vec{k}\cdot\vec{r}}\, \mathrm{d}k_{z1}\, \mathrm{d}k_{z2}, \tag{34}$$

where the integration paths are those in Table 3. The asymptotic evaluation of this integral $\overline{\overline{g}}_{0,0}(\vec{r}) \sim g^v(\vec{r})$ is performed by a generalization of the 1D VdW procedure to 2D integrals. The VdW method involves mapping the *given* integrand (both phase and amplitude) onto the simplest *canonical* integrand that accommodates the relevant configuration of critical points. Reduction to the canonical form is accomplished by selectively adding and subtracting "regularizing" portions in the integrand which, as mentioned earlier, can involve an *arbitrary* number of poles. In [10], regularization has been carried out for only that $(p, q)$ pole which is closest to the SP. The results shown in Table 4 involve a canonical function $T(a, b, w)$ that extends over a limited region $Q$ in the $(k_{z1}, k_{z2})$ spectral domain, large enough to accommodate the asymptotic isolation of the SP and poles at its boundary, and with its center defined by SP-pole coalescence. The appealing structure of $T(a, b, w)$ is based on a modification of a less explicit four-parameter function introduced in [17]. Similar canonical functions have also been employed and discussed in [18,19] for description of double diffraction problems. The chosen normalization ensures that $T(a, b, w)$ tends to unity for large values of the parameters $a$ and $b$ (i.e., for poles far from the SP). The numerical evaluation of $T(a, b, w)$ can be performed as in [18–20] in terms of standard *generalized Fresnel integrals* [21,22]. Large values of the arguments $a_q$ and $b_p$, away from the SP, define the onset of the non-uniform regime where $T \to 1$. This criterion determines the extent of the local region $Q$ mentioned at the beginning of this section, which permits patching from the locally uniform asymptotics inside $Q$ onto the non-uniform asymptotics exterior to $Q$.

The vertex-diffracted $g^v(\vec{r})$ in Table 4 incorporates the transition from a vertex-dominated spherical wave to an edge-dominated cylindrical wave, and it compensates for the discontinuities across the SBCs of edge diffracted rays $\beta_{1,q} = \beta_1$ and $\beta_{2,p} = \beta_2$; the respective parameters $a_q$ and $b_p$ vanish there. The asymptotically dominant terms in the compensation mechanism at $\beta_{1,q} = \beta_1$ are those involving $F(a_q^2)$, and the corresponding reduced form of $T(a_q, b_p, w)$, for $\beta_2 \neq \beta_{2,p}$, behaves like $F(a_q^2)$. Analogous considerations apply to $\beta_{2,p} = \beta_2$. At the simultaneous intersection of the edge diffracted conical $\mathrm{SBC}_{1,2}$ and the truncated FW planar $\mathrm{SB}_{1,2}$ (see Fig. 3), both $a_q$ and $b_p$ vanish; the corresponding $T(a_q, b_p, w)$ function transforms the vertex-induced field locally into a plane wave to match the FW. Finally, since the $F$ and $T$ functions tend to unity for large $a_q$ and $b_p$, i.e., far from conical shadow boundaries, the quantities $[1 - F]$ and $[T(a_q, b_p, w) - F(a_q^2) - F(b_p^2) + 1]$ they are of asymptotic order $(kr)^{-1}$, whence the dominant asymptotic term is $\mathrm{j}B_1(\bar{k}_{z1s}) B_2(\bar{k}_{z2s})$. Complete analytic tracking of this uniform asymptotic matching in overlapping shadow boundary transition regions is demonstrated in [23]. Results for the vector electromagnetic field are obtained from the above by substituting for the spectral Green's function of the potential the spectral dyadic Green's function of the field (explicit expressions are found in [10]).

## 3.6. Directive elements and array far zone field

When the observer is in the far zone of each element of an actual array with element pattern function $\vec{Q}(\beta_1, \beta_2)$, but in the Fresnel zone of the total array, the field of the actual array may be approximated through multiplication

of the AGF by $\vec{Q}(\beta_1, \beta_2)$. When observing in the far zone of the total array (i.e., $r > 2D^2/\lambda$, where $D$ is the largest array dimension), the amplitude of the AGF can be identified as the familiar array factor in the principle of pattern multiplication [24]. Under these conditions, the angular transition regions and shadow boundaries between the propagating FW and the FW-induced edge diffracted rays disappear. The far field pattern is thus given by the combination of the non-uniform diffracted rays from the four vertices, analogous to what occurs for GTD-scattering by a metallic rectangular plate illuminated by a plane wave [25], where the singularities of the diffracted rays at the shadow boundaries cancel, and the field everywhere is well-behaved.

## 4. Numerical results

We now present numerical results which illustrate the application and accuracy of the asymptotics in Section 3. In Section 4.1, we test the accuracy of the AGF. In Section 4.2, we consider application of the AGF to a typical side-wall slotted waveguide resonant array. Finally, we briefly describe how the high-frequency AGF can be incorporated in an integral equation analysis for determining the element currents.

### *4.1. Validation test*

Numerical tests have been performed on a "large" square array of dipoles in order to validate the high-frequency formulation in Table 4. Next, we use the AGF to calculate co-polar and cross-polar components due to a $50 \times 50$ element, side-wall slotted waveguide resonant array in broadside configuration. For convenient determination of the cross-polar components, and to gain physical insight, we decompose the total AGF into two $25 \times 50$ sub-array AGFs, as shown in Fig. 5. The two sub-arrays have interelement periods of $d_1 = 1.4\lambda, d_2 = 0.5\lambda$ (one being shifted by $0.7\lambda$ with respect to the other), therefore radiating three FWs each; the slots of each sub-array are tilted through $+10^\circ$ and $-10^\circ$, respectively (see Fig. 5a). *Co-polar*, and *cross-polar* components of the electric field are calculated in Fig. 5b and c, on the $E$-plane at a radial distance $r = 50\lambda$. An element-by-element summation over the contribution from each dipole serves as a reference. From a variety of near field scans carried out for different array parameters and dipole orientations, we have selected one example because of space limitations. The quality of the analytic–numerical comparison in the example of Fig. 4 is typical of what we have found throughout. The dashed curve denotes the radiated field without vertex contributions, thereby illustrating how the vertex-diffracted waves compensate for the disappearance of the edge diffracted waves at their SBCs, rendering the total radiated field continuous.

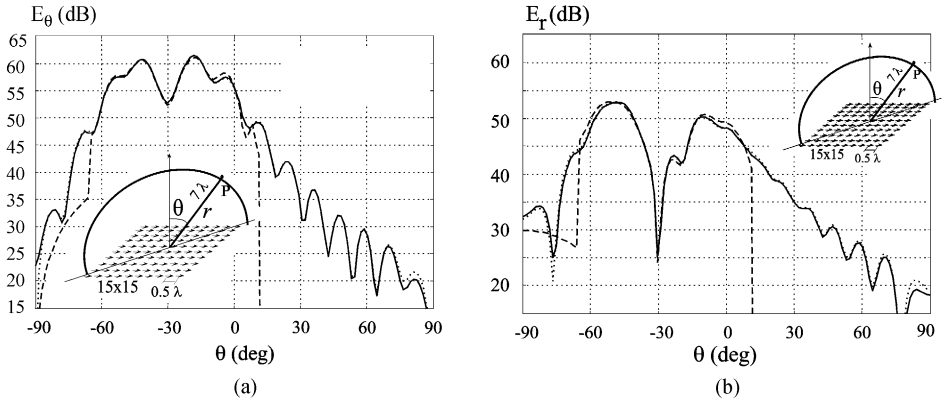


Fig. 4. Electric field for a rectangular array ($\gamma_1 = \gamma_2 = 2/\lambda$). The solution is based on (18) and Table 4. Scan close to a vertex in a plane normal to the array and at 45° between the edges, containing the array normal. Asymptotic solution (continuous curve), reference solution (dotted curve), asymptotic solution without vertex contribution (dashed curve) (a) angular and (b) radial component.

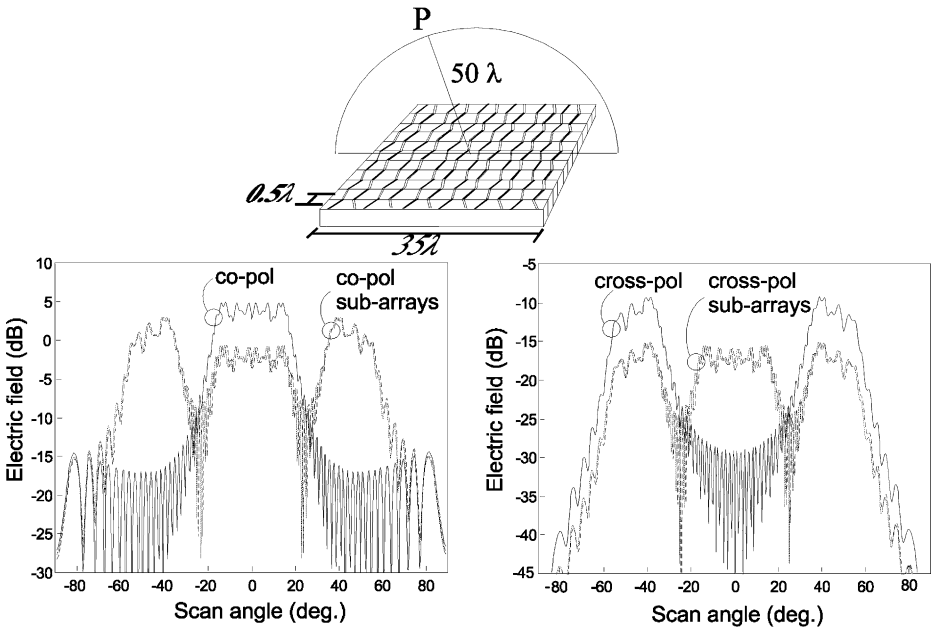


(a) (b)

Fig. 5. Actual array as a superposition of two sub-arrays. Co-polar components (a) and cross-polar components (b) of the electric field along the $E$-plane at a distance $r = 50\lambda$ from the center of the array. Solid curves: total radiated field. Dashed and dotted curves: sub-array fields. Summing the two sub-array co-polar components give the main beam of the total field radiated by the array. Vice versa, summing the two sub-array cross-polar components cancels the main beam and only the lateral lobes remain. The results from the reference element-by-element solution was superimposed with those from the asymptotics so that they have not been reported.

Strong cross-polar components arise from the slot tilts which give rise to equivalent magnetic currents oriented along $z_1$. The dotted and dashed curves represent the field radiated by the sub-arrays, while the solid curves represent their sum to synthesize the total field. Each sub-array field has three maxima, tied to the three FWs $(p, q) = (0, -1)$, (0,0), and (0,1). In Fig. 5b, the two sub-array *co-polar* components are summed to yield the broadside beam of the total field radiated by the array. The side lobes cancel as expected since the original array interelement period is $d_1 = 0.7\lambda$. The cancellation is attributed to the $0.7\lambda$ shift between the two arrays which, in the side lobe directions, produces beams in exact opposite phase. Vice versa, in Fig. 5c, when the sub-array *cross-polar* components are summed, the main beam cancels and only the side lobes remain. Because the slots of the two sub-arrays are tilted in opposite directions, they radiate main beam cross-polar fields in opposite phase; the lateral cross-polar lobes remain because the sub-array side lobes now have the same phase. This shows that the cross-polar lobes are oriented along directions coincident with the odd-order FWs ($q = -1, 1$). Increasing the observer distance, the main beam becomes more prominent, the valleys become deeper, with the cancellation effects intact.

### *4.2. Use of the AGF in a full-wave array analysis*

The rectangular AGF can be used as the basic constituent for structuring a full-wave analysis of practical arrays. The usual perturbation approximation, using the windowing scheme [1,2], may lead to inaccuracies in predicting the effects of truncation, especially when studying aperture arrays on ground planes. A more rigorous scheme, not affected by a priori assumptions and proposed in [26,27], is based on the method of moments (MoM) solution of two decoupled integral equations (IEs). The first IE is that pertinent to the infinite array (IAIE). The second IE, denoted by Fringe IE (FIE) is obtained by subtracting the infinite array IE from the IE of the actual, finite array. The

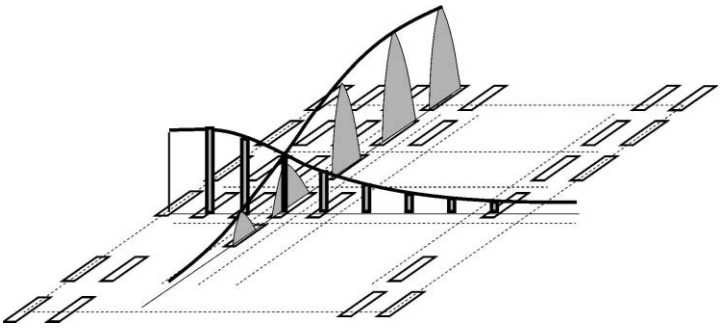

Fig. 6. Global basis functions for expanding the unknown of the FIE. The basis functions are shaped as FW induced edge diffracted rays which modulate resonant functions on the slots.

total solution is obtained by the superposition of the solution of the IAIE plus the solution of the FIE. In solving the IAIE one can use an accurate representation of the periodic AGF, including a large number of EFW. However, the solution of the IAIE does not require substantial computational effort because of the periodicity hypothesis. The unknown function of the FIE is the difference between the exact solution of the finite array and that of the associated infinite array. This unknown function has an intrinsic diffractive nature, thus allowing its simple and efficient representation in terms of diffracted rays associated with truncated FWs. The forcing term in this FIE is the field radiated by the complementary portion of the actual array with currents equal to those of the infinite array. In this context, the high-frequency AGF formulation exhibits a double advantage. First, it allows substantial saving of calculation time in describing the forcing term of the FIE. Next, it provides the guideline for defining global basis functions, in terms of which to efficiently expand the FIE unknown, thus providing reduction of the matrix size to be inverted. The basis functions for the FIE unknowns are defined using the analytic expressions of the diffracted ray to modulate resonant type functions defined on the slots (see Fig. 6). The number of unknowns of the problem is therefore like the number of significant FW-modulated edge diffracted rays, which in most cases are those excited by the propagating and the first EFW. This means that the FIE-matrix to be inverted is usually $8 \times 8$ regardless of the number of elements of the rectangular array.

For illustration, consider a resonant-slot array on an infinite ground plane. The array is comprized of $20 \times 20$ $y$-oriented slots with length $0.5\lambda$ and width $0.005\lambda$. The interelement periods are $d_x = 0.5\lambda$ and $d_y = 0.7\lambda$ and

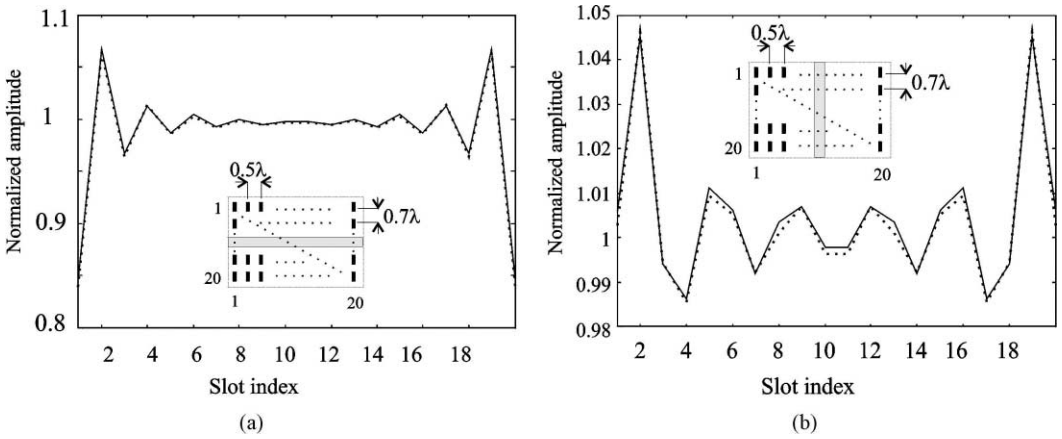


Fig. 7. Normalized amplitude of the magnetic currents versus the slit index for an array of $20 \times 20$ slots: $d_1 = 0.7\lambda$, $d_2 = 0.5\lambda$, broadside beam. Dots: element-by-element MoM solution; solid curve: asymptotic AGF-based solution. (a) 10th row, (b) 10th column.

the slots are fed with uniform amplitude and phase. The curves show the amplitude of the normalized magnetic currents as a function of the slot index on a central row (Fig. 7a) or column (Fig. 7b) of the array. The solid curve pertains to the method described above, while the dotted curve states results obtained from a conventional element-by-element MoM, assuming a single resonant-type basis function on each slot. Since the slots are thin, the global distribution is adequately described by only one sample per slot; the samples are connected by straight segments to highlight the slot-by-slot oscillation around the solution for the infinite array (which is unity due to the normalization). This oscillation, already observed by Hansen and Gammon [28], who described it on the basis of a Gibbsian model, is established by the interference between each FW aperture field and its corresponding diffracted ray. We emphasize that although the FW-diffraction method implies the solution of an $8 \times 8$ linear system versus the $400 \times 400$ linear system for the element-by-element MoM approach, the results are almost coincident.

## 5. Conclusion

In this paper, a high-frequency formulation for the AGF of a periodic rectangular array of linearly phased parallel dipoles has been developed and utilized as the base for an array-matched generalized GTD which extends the concepts of conventional GTD for smooth configurations. The rectangular array has been parameterized in terms of the phenomenologies of the constituent infinite sectoral arrays. Each sectoral array has been decomposed into the SIAs corresponding to the two non-truncated sector edges, and the vertex contribution. The AGF is obtained first by direct summation over the contributions from the individual radiators, and is then globally restructured via the 2D Poisson sum formula into spatial domain integrals which are asymptotically dominated by critical points in the integration domain. These points are categorized depending on the FWs and of the corresponding FW-modulated diffracted rays, which arise from FW diffraction at the sectoral array edges and vertex. The spectral domain version of the 2D Poisson formula can be similarly parameterized in terms of critical spectral points and relevant wave contributions. Different species of spectral poles define the various species of propagating and EFWs. The other critical points in the double spectral integral define the asymptotic behavior of the edge and vertex-diffracted rays, and the confluence of these critical points determines a variety of locally uniform transition regions for truncated edge diffracted and vertex-diffracted waves. The uniform asymptotics governing this phenomenology is physically appealing, numerically accurate, and efficient, owing to the rapid convergence of both the FW series and the series of corresponding FW-modulated diffracted fields away from the array plane. The use of this asymptotic construct not only speeds up the AGF calculations, but also provides the basic guidelines for the formulation of a hybrid method where FW-modulated diffracted rays are used as basis functions in an MoM scheme.

## Acknowledgements

F. Capolino, and S. Maci acknowledge partial support by the European Space Agency (ESA-ESTEC, 2200 AG Noordwijk, The Netherlands) and by the Agenzia Spaziale Italiana (ASI). F. Capolino acknowledges the Italian Research National Council (CNR) for a Grant awarded in 1998–1999, to conduct research at Boston University. L.B. Felsen acknowledges partial support by the US–Israel Binational Science Foundation, Jerusalem, Israel, under Grant 95-00399, and from ODDR&E under MURI Grants ARO DAAG55-97-1-0013 and AFOSR F49620-96-1-0028.

## References

[1] A. Ishimaru, R.J. Coe, G.E. Miller, W.P. Geren, Finite periodic approach to large scanning array problems, IEEE Trans. Antenn. Propagat. 33 (1985) 1213–1220.

[2] A. Skrivervik, J. Mosig, Finite planed array of microstrip patch antennas: the infinite array approach, IEEE Trans. Antenn. Propagat. 40 (1992) 579–582.

[3] P.-S. Kildal, Diffraction corrections to the cylindrical wave radiated by a linear array feed of a cylindrical reflector antenna, IEEE Trans. Antenn. Propagat. 32 (1984) 1111–1116.
[4] L.B. Felsen, L. Carin, Diffraction theory of frequency and time domain scattering by weakly aperiodic truncated thin wire gratings, J. Opt. Soc. Am. 11 (1994) 1291–1306.
[5] L.B. Felsen, E. Gago Ribas, Ray theory for scattering by two-dimensional quasi-periodic plane finite arrays, IEEE Trans. Antenn. Propagat. 44 (1996) 375–382.
[6] L. Carin, L.B. Felsen, T.-T. Hsu, High-frequency fields excited by truncated arrays of non-uniformly distibuted filamentary scatterers on an infinite dielectric grounded slab: parametrizing (leaky mode)–(Floquet mode) interaction, IEEE Trans. Antenn. Propagat. 44 (1996) 1–11.
[7] F. Capolino, M. Albani, S. Maci, R. Tiberio, High-frequency analysis of an array of line sources on a truncated ground-plane, IEEE Trans. Antenn. Propagat. 46 (1998) 570–578.
[8] F. Capolino, M. Albani, S. Maci, L.B. Felsen, Frequency domain Green's function for a planar periodic semi-infinite phased array. Part I. Truncated Floquet wave formulation, IEEE Trans. Antenn. Propagat. 48 (2000) 67–74.
[9] F. Capolino, M. Albani, S. Maci, L.B. Felsen, Frequency domain Green's function for a planar periodic semi-infinite phased array. Part II. Diffracted wave phenomenology, IEEE Trans. Antenn. Propagat. 48 (2000) 75–85.
[10] F. Capolino, S. Maci, L.B. Felsen, Green's function for a planar phased sectoral array of dipoles, Radio Sci. 35 (2000) 579–593.
[11] A. Papoulis, The Fourier Integral and its Applications, McGraw-Hill, New York, 1962.
[12] A. Papoulis, Probability, Random Variables and Stochastic Processes, McGraw-Hill, New York, 1984.
[13] L.B. Felsen, N. Marcuvitz, Radiation and Scattering of Waves, Prentice-Hall, Englewood Cliffs, NJ, 1973, also IEEE Press, Piscataway, NJ, 1994.
[14] S. Maci, F. Capolino, L.B. Felsen, Three-dimensional Green's function for planar rectangular phased dipole arrays, Technical Report No. AM-99-007, Department of Aerospace and Mechanical Engineering, Boston University, 1998.
[15] B.L. Van der Waerden, On the method of saddle points, Appl. Sci. Res. B 2 (1951) 33–45.
[16] R.G. Kouyoumjian, P.H. Pathak, A uniform geometrical theory of diffraction for an edge in a perfectly conducting surface, Proc. IEEE 62 (1974) 1448–1461.
[17] K.H. Hill, A UTD solution to the EM scattering by the vertex of a perfectly conducting plane angular sector, Ph.D. Thesis, Department of Electrical Engineering, Ohio State University, 1990.
[18] F. Capolino, M. Albani, S. Maci, R. Tiberio, Diffraction from a couple of coplanar, skew wedges, IEEE Trans. Antenn. Propagat. 45 (1997) 1219–1226.
[19] M. Albani, F. Capolino, S. Maci, R. Tiberio, Diffraction at a thick screen including corrugations on the top face, IEEE Trans. Antenn. Propagat. 45 (1997) 277–283.
[20] F. Capolino, S. Maci, Simplified, closed-form expressions for computing the generalized Fresnel integral and their application to vertex diffraction, Microw. Opt. Technol. Lett. 9 (1995) 32–37.
[21] F. Capolino, S. Maci, Uniform high-frequency description of singly, doubly, and vertex-diffracted rays for a plane angular sector, J. Wave Appl. 10 (1996) 1175–1197.
[22] D.S. Jones, A uniform asymptotic expansion for a certain double integral, Proc. Roy. Soc. Edinburg A 69 (1971) 205–226.
[23] F. Capolino, S. Maci, L. Felsen, Uniform high-frequency formulation for diffraction at the vertex of a planar phased sectoral array of dipoles, IEEE Trans. Antenn. Propagat, in preparation.
[24] J.D. Kraus, Antennas, McGraw-Hill, New York, 1988.
[25] S. Maci, R. Tiberio, A. Toccafondi, Diffraction at a plane angular sector, J. Wave Appl. 8 (1994) 1247–1276.
[26] A. Neto, S. Maci, G. Vecchi, M. Sabbadini, A truncated Floquet wave diffraction method for the full-wave analysis of large phased arrays: basic principles and 2D case, IEEE Trans. Antenn. Propagat. 48 (2000).
[27] A. Neto, S. Maci, G. Vecchi, M. Sabbadini, A truncated Floquet wave diffraction method for the full-wave analysis of large phased arrays: generalization to the 3D case, IEEE Trans. Antenn. Propagat. 48 (2000).
[28] R.C. Hansen, D. Gammon, A Gibsian model for finite scanned arrays, IEEE Trans. Antenn. Propagat. 44 (1996) 243–248.